

Topological orbital superfluid with chiral d -wave order in a rotating optical lattice

Ningning Hao,^{1,*} Huaiming Guo,² and Ping Zhang^{3,4,†}

¹Anhui Province Key Laboratory of Condensed Matter Physics at Extreme Conditions,
High Magnetic Field Laboratory, Chinese Academy of Sciences, Hefei 230031, Anhui, China

²Department of Physics, Beihang University, Beijing 100191, China

³Institute of Applied Physics and Computational Mathematics, Beijing 100088, China

⁴Beijing Computational Science Research Center, Beijing 100193, China

Topological superfluid is an exotic state of quantum matter that possesses a nodeless superfluid gap in the bulk and Andreev edge modes at the boundary of a finite system. Here, we study a multi-orbital superfluid driven by attractive s -wave interaction in a rotating optical lattice. Interestingly, we find that the rotation induces the inter-orbital hybridization and drives the system into topological orbital superfluid in accordance with intrinsically chiral d -wave pairing characteristics. Thanks to the conservation of spin, the topological orbital superfluid supports four rather than two chiral Andreev edge modes at the boundary of the lattice. Moreover, we find that the intrinsic harmonic confining potential forms a circular spatial barrier which accumulates atoms and supports a mass current under injection of small angular momentum as external driving force. This feature provides an experimentally detectable phenomenon to verify the topological orbital superfluid with chiral d -wave order in a rotating optical lattice.

I. INTRODUCTION

Orbital degrees of freedom play a significant role to produce various exotic quantum states in complex condensed-matter systems, such as high temperature superconductors and quantum magnetic insulators. Recent experimental realizations of multi-orbital systems with ultra-cold atoms¹⁻⁴ have promoted the theoretical studies of high orbital physics in optical lattices, where a series of exotic quantum states have been proposed⁵⁻¹¹. Among them, one of remarkable characteristics is that the orbital hybridization can play the same role as spin-orbital coupling or artificial gauge fields which are the key ingredient to drive topologically insulating or superconducting states^{12,13}. Therefore, topologically nontrivial many-body states can be implemented in multi-orbital systems in the absence of spin-orbital couplings. There exist several methods to induce the orbital hybridization in the context of cold atom systems, including many-body interaction effect⁵, lattice shaking¹⁴⁻¹⁷, and local rotation¹⁸. The relevant quantum states including topological semimetal⁵ and topological band insulators^{10,15,20,21} have been proposed.

Recently, the superfluid of bosons with chiral odd-frequency orders, i.e., $p + ip$ -wave and $f + if$ -wave, have been experimentally realized in multi-orbital cold-atom systems^{2,22,23}. For the fermions, however, it is still a big challenge to realize the superfluid states with chiral odd-frequency orders, because the atom loss is strong near the Feshbach resonance in high-frequency channels²⁴. Theoretically, thanks to the Rashba spin-orbital couplings, the topological superfluids of fermions with chiral odd-frequency orders have been proposed to emerge in s -wave channel of the Feshbach resonance²⁵⁻²⁸. In comparison with well-studied chiral odd-frequency superfluids of fermions, the superfluids of fermions with chiral even-frequency orders are rarely studied, and only some candidate materials are proposed to have the chiral even-frequency orders due to the unconventional superconducting pairing in condensed-matter systems²⁹⁻³². More recently, a checkerboard lattice in a periodic Floquet driving field was proposed to support the chiral d -wave superfluid, where the sublattice degrees of freedom plays a key role and the periodic Floquet driving field induces the hybridization of two sublattices³³. In this paper, we propose that a superfluid state of fermions with a chiral d -wave order can be implemented in a rotating multi-orbital optical lattice. In our proposal, the key ingredients to drive the underlying nontrivial topology of the multi-orbital superfluid state with a chiral d -wave order come from the two orbitals that are the counterparts of spin degrees of freedom in spin-orbital coupling, and the inter-orbital hybridization is induced by the local rotation with same frequency for every individual lattice site, which can be experimentally realized¹⁸. Interestingly, different from conventional chiral d -wave topological superfluid which supports two chiral Andreev edge modes at the boundary of the system, the topological orbital superfluid here supports four chiral Andreev edge modes due to the conservation of spin. More importantly, we find that the spatial barrier structure spontaneously formed by the intrinsic harmonic confining potential separates the trivial and nontrivial superfluid states, accumulates cold atoms and supports a mass current under injection of small angular momentum as the external driving force. These features can be experimentally adopted to verify the topologically non-trivial superfluid states. In comparison with the chiral p -wave and f -wave topological superconductor and superfluid^{25,26,28,34-40}, where the spin-orbital couplings are essential, the chiral d -wave topological superfluid here only requires the orbital hybridization. Therefore, our proposal provides a possible route to explore topological superfluids with chiral d -wave order in multi-orbital cold-atom systems.

The paper is organized as follows. In section II, we discuss the implementation of the multi-orbital system with a specific configuration of laser beams, and construct the effective Hamiltonian to describe the multi-orbital system. In section III, we study the homogeneous superfluid state with self-consistent mean-field approximation, and discuss the topological properties of the homogeneous superfluid state. In section IV, we discuss the inhomogeneous superfluid state modulated by the harmonic

TABLE I: The parameters of the electric fields of four laser beams shown in Fig. 1(a).

j	E_{j0}	\vec{e}_j	\vec{k}_j	ω_j	φ_j
1	ϵ_1	(1, 0, 0)	$(k_L/2, 0)$	ω_0	0
2	ϵ_1	(0, 1, 0)	$(0, k_L/2)$	ω_0	0
3	ϵ_2	(0, 0, 1)	$(k_L/2, k_L/2)$	ω_0	0
4	ϵ_2	(0, 0, 1)	$(k_L/2, -k_L/2)$	ω_0	0

confining potential. In section V, we discuss the experimental scheme and present a brief summary.

II. OPTICAL LATTICE AND MODEL

We consider a balanced mixture of fermion atoms with two internal states labeled by the spin index σ . The atoms are loaded in an isotropic 2D square optical lattices. To introduce the couplings between different p orbital bands, one effective approach is to rotate the optical lattice with same rotation frequency Ω_z for every individual lattice site¹⁸. An alternative approach would be to directly couple the states with a drive laser¹⁹. Finally, the trapped atoms are turned close to a Feshbach resonance to produce attractive s -wave interactions. The lattice potential takes the form,

$$V(x, y) = V_1[\cos k_L x + \cos k_L y] + 2V_2 \cos k_L x \cos k_L y. \quad (1)$$

Here, V_1 and V_2 are the optical lattice potentials and k_L is the wave-vector of laser fields. The realization of lattice potential $V(x, y)$ in Eq. (1) has been proposed for the case $V_2/V_1 > 1/2$ ⁵. Here, we consider the case $V_2/V_1 < 1/2$, and the configuration of optical lattices under the condition $V_2/V_1 < 1/2$ can be implemented through four retro-reflected laser beams as shown in Fig. 1(a). The electric field generated by each laser beam is

$$\vec{E}_j(\vec{r}, t) = E_{j,0} \vec{e}_j \cos(\vec{k}_j \cdot \vec{r}_j) e^{-i(\omega_j t + \varphi_j)}, \quad (2)$$

where \vec{e}_j , ω_j , and φ_j are the polarization vector, the frequency, and the phase of the laser field, respectively. The parameters for each laser beams are summarized in Table I. The corresponding light-shift potential is

$$V(x, y) = -\chi \left| \sum_j \vec{E}_j(\vec{r}, t) \right|^2, \quad (3)$$

with χ denoting the real part of the polarizability. By adopting the parameters in Table I, we can get the lattice potential shown in Eq.(1) with an irrelevant constant shift $V_0 = -\chi(\epsilon_1^2 + \epsilon_2^2)$. Here, $V_1 = -\chi(\epsilon_1^2/2 + \epsilon_2^2)$, and $V_2 = -\chi\epsilon_2^2/2$. The condition $V_2/V_1 < 1/2$ can be achieved for arbitrary nonzero ϵ_1 and ϵ_2 and blue detuning with $\chi < 0$. Here, we set $V_1 = 1.2E_R$ and $V_2 = 0.4E_R$. $E_R = \frac{\hbar^2}{2ma^2}$ is the recoil energy and a is the lattice constant.

The contour of $V(x, y)$ is shown in Fig. 1(b). The lowest four band structures from the plane-wave expansion approximation upon the potential $V(x, y)$ in Eq. (1) are shown in Fig. 1(d). It is straightforward to check that the splitting between two middle p_x and p_y bands off the high-symmetry point are induced by the coupling to the higher $d_{x^2-y^2}$ band⁵. Consider the three orbitals of p_x , p_y and $d_{x^2-y^2}$ shown in Fig. 1(e), a tight-binding (TB) Hamiltonian can be constructed to described the band structures of the fermionic square lattice, i.e.,

$$H_{tb} = H_d + H_p + H_{dp}, \quad (4)$$

with

$$H_d = \sum_{\langle i,j \rangle \sigma} [-t_{dd} + (\delta - \mu_i)\delta_{ij}] d_{i,\sigma}^\dagger d_{j,\sigma}, \quad (5)$$

$$\begin{aligned} H_p = & - \sum_{i\sigma, l=x,y} \mu_i p_{l,i,\sigma}^\dagger p_{l,i,\sigma} + i\hbar\Omega_z \sum_{i\sigma} p_{x,i,\sigma}^\dagger p_{y,i,\sigma} + H.c. \\ & + t_{pp} \sum_{i\sigma, l=x,y} p_{l,i,\sigma}^\dagger p_{l,i+e_l,\sigma} + H.c. \\ & - t'_{pp} \sum_{i\sigma, l=x,y, \bar{l}=-l} p_{l,i,\sigma}^\dagger p_{l,i+e_{\bar{l}},\sigma} + H.c., \end{aligned} \quad (6)$$

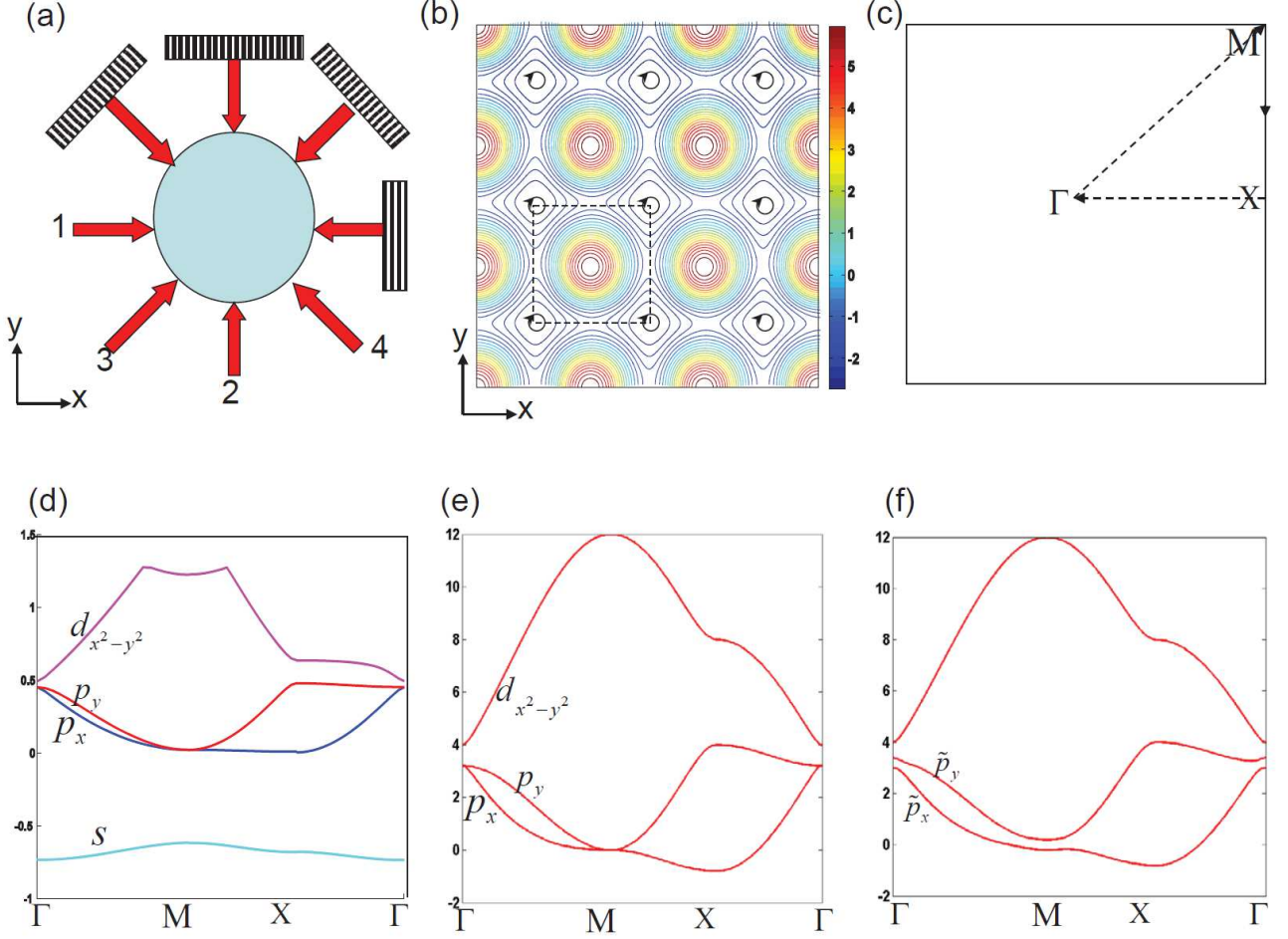


FIG. 1: (Color Online) (a) Four retro-reflected laser beams are adopted to create the lattice potential in Eq. (1). (b) The contour of the lattice potential forms a two-dimensional optical lattice, and the atoms are trapped at the minima of the potential. The small circle with arrow at each minimum represents the on-site rotation. Here, $V_1 = 1.2E_R$ and $V_2 = 0.4E_R$ (c) The Brillouin zone and high-symmetry points. (d) The single-particle energy spectrum along high-symmetry lines in the unit of E_R for the four lowest bands through plane wave expansion calculation about the lattice potential. (e) and (f) The single-particle energy spectrum along high-symmetry lines from the tight-binding Hamiltonian in Eq.(4) without and with on-site rotation. To guarantee the consistence of the energy scales between the bands from plane wave expansion calculation about the lattice potential in (d) and the bands from tight-binding calculations in (e) and (f), the energy is measured in the unit of t_{pp} with $t_{pp} = 0.1E_R$ in (e) and (f). Other parameters are $t_{dd} = 1$, $t_{pd} = 1$, $t'_{pp} = 0.2$, $\delta = 6.4$, $\mu_0 = -1.6$, $V_t = 0$ and $\hbar\Omega_z = 0$ in (e) and $\hbar\Omega_z = 0.2$ in (f).

$$H_{dp} = t_{pd} \sum_{i\sigma, l=x,y} [p_{l,i+e_l,\sigma}^\dagger d_{i,\sigma} - p_{l,i-e_l,\sigma}^\dagger d_{i,\sigma}] + H.c. \quad (7)$$

Here, $\mu_i = \mu_0 + V_{trap}(i_x, i_y)$ with

$$V_{trap}(i_x, i_y) = V_t \left[\left(i_x - \frac{N_x + 1}{2} \right)^2 + \left(i_y - \frac{N_y + 1}{2} \right)^2 \right] \quad (8)$$

being the weak harmonic confining potential to stabilize the optical lattice. $p_{x/y,i,\sigma}^\dagger$ and $d_{i,\sigma}^\dagger$ are the fermion creation operators for atoms in the relevant p_x , p_y and $d_{x^2-y^2}$ orbitals. We first set $V_t = 0$ to simplify the discussions and recover it later. Note that all the energy scales are measured in the unit of t_{pp} as explained in the caption of Fig. 1 in the following parts of the paper if not special specified. The energy spectra of TB Hamiltonian in Eq. (4) are shown in Figs. 1(e) and 1(f). It can be found that

the TB Hamiltonian in Eq. (4) gives a good description of the band structures of lattice potential, and the on-site rotation in the second term in Eq. (6) induces the orbital hybridization to break the degeneracy of p_x and p_y bands around the Γ and M points shown in Fig. 1(c).

When the fermion atoms are loaded into the two p_x and p_y bands, the attractive s -wave interactions from the Feshbach resonance give the two-orbital attractive Hubbard interactions as follows⁴¹,

$$H_{int} = U \sum_{il} n_{il\uparrow} n_{il\downarrow} - \frac{J}{2} \sum_i [2\mathbf{S}_{ix} \cdot \mathbf{S}_{iy} + \frac{1}{2} n_{ix} n_{iy}] + \frac{J}{2} \sum_i n_{ix} n_{iy} + J_{\Delta} \sum_i p_{ix\uparrow}^{\dagger} p_{ix\downarrow}^{\dagger} p_{iy\downarrow} p_{iy\uparrow} + H.c. \quad (9)$$

Here, the first term is the intra-orbital attractive interaction, and the second term is the Hund's coupling with the spin operator $\mathbf{S}_{il} = \frac{1}{2} p_{il,\alpha}^{\dagger} \sigma_{\alpha\beta} p_{il,\beta}$ and $l = x, y$. U and J take the following forms,

$$U = 4\pi\hbar^2 a_s / m \int dr |\omega_{x/y}(r)|^4, \quad (10)$$

$$J = 4\pi\hbar^2 a_s / m \int dr |\omega_x(r)|^2 |\omega_y(r)|^2. \quad (11)$$

Here, a_s is the s -wave scattering length with negative value, i.e., $a_s < 0$. $\omega_{x/y}(r)$ are the Wannier functions of $p_{x/y}$ orbitals. The third term in Eq. (9) is the inter-orbital attractive interaction with $n_{il} = n_{il,\uparrow} + n_{il,\downarrow}$. The fourth term is the pair hopping term. Furthermore, we have $J = 2U/3$ and $J_{\Delta} = U/3$ ⁴¹. Note that the Hund's coupling and inter-orbital interaction have same amplitudes, which are different from the electron system. The interaction terms shown in Eqs.(9)-(11) are obtained under the harmonic approximation. It is shown that the an-harmonicity of the optical lattice can affect the properties of the multi-orbital system^{42,43}. In particular, the intra-orbital interaction U_{xx} is not equal to U_{yy} , and the inter-orbital interaction J is off $2U_{xx}/3$. Such imbalance can induce the modulations of superfluid order parameters. However, the topological superfluid is robust against such small modulations, because nontrivial topology is the global feature of superfluid. For simplification, we neglect the irrelevant an-harmonic effects in the present work.

III. HOMOGENEOUS SUPERFLUID STATES WITH CHIRAL D-WAVE ORDER

Now, we turn to consider the homogeneous superfluid state with $V_t = 0$ in Eq. (8) and the superfluid state is driven by the attractive interaction in Eq. (9). The spin-singlet superfluid pairing operators are defined as

$$\hat{\Delta}_{s,ll'}(k) = \sum_{\sigma\sigma'} \frac{[i\sigma_y]_{\sigma\sigma'}}{4} [p_{l,k\sigma} p_{l',-k\sigma'} + p_{l',k\sigma} p_{l,-k\sigma'}]. \quad (12)$$

Then, we have

$$H_{int} = U \sum_l \hat{\Delta}_{s,ll}^{\dagger} \hat{\Delta}_{s,ll} + J_{\Delta} \sum_{l \neq l'} \hat{\Delta}_{s,ll}^{\dagger} \hat{\Delta}_{s,l'l'} + 2J \sum_{l > l'} \hat{\Delta}_{s,ll'}^{\dagger} \hat{\Delta}_{s,ll'} \quad (13)$$

with

$$\hat{\Delta}_{s,ll'} = \sum_k \hat{\Delta}_{s,l'l'}(k). \quad (14)$$

Note that the spin-triplet pairing parts disappear, because the Hund's coupling and inter-orbital interaction have the same amplitudes. Through the mean-field approximation, $\Delta_{s,ll'} = \langle \hat{\Delta}_{s,ll'} \rangle$, H_{int} can be decoupled to be

$$H_{int}^p = \sum_{l,k} (U \Delta_{s,ll} + J_{\Delta} \Delta_{s,\bar{l}}) \hat{\Delta}_{s,ll}^{\dagger}(k) + H.c. + \sum_k 2J \Delta_{s,xy} \hat{\Delta}_{s,xy}^{\dagger}(k) + H.c. + h_{con} \quad (15)$$

with

$$h_{con} = -U \sum_l |\Delta_{s,l}|^2 - 2J |\Delta_{s,xy}|^2 - 2J_\Delta \text{Re}(\Delta_{s,xx} \Delta_{s,yy}^*). \quad (16)$$

The homogeneous superfluid state can be described by the mean-field Hamiltonian in the Nambu basis: $\Psi(k) = [d_{k\uparrow}, p_{x,k\uparrow}, p_{y,k\uparrow}, d_{k\downarrow}^\dagger, p_{x,k\downarrow}^\dagger, p_{y,k\downarrow}^\dagger, d_{k\downarrow}, p_{x,k\downarrow}, p_{y,k\downarrow}, d_{k\uparrow}^\dagger, p_{x,k\uparrow}^\dagger, p_{y,k\uparrow}^\dagger]^t$,

$$H_{mf} = \sum_k \frac{1}{2} \Psi^\dagger(k) \begin{bmatrix} H_{tb}(k) & \Delta \\ \Delta^\dagger & -H_{tb}^*(-k) \\ & H_{tb}(k) & -\Delta \\ & -\Delta^\dagger & -H_{tb}^*(-k) \end{bmatrix} \Psi(k) + C. \quad (17)$$

Here, C is an operator-independent constant term. Δ is a 3×3 matrix and takes the following form,

$$\Delta = \begin{bmatrix} 0 & 0 & 0 \\ 0 & U\Delta_{s,xx} + J_\Delta\Delta_{s,yy} & 2J\Delta_{s,xy} \\ 0 & 2J\Delta_{s,xy} & U\Delta_{s,yy} + J_\Delta\Delta_{s,xx} \end{bmatrix}. \quad (18)$$

The mean-field Hamiltonian in Eq. (17) can be self-consistently solved with respect to the minimum of ground state energy, i.e.,

$$E_g = h_{con} - \frac{1}{4\pi^2} \sum_{n=1}^3 \int d^2\mathbf{k} [|E_n^{(s)}(k)| - |E_n^{(0)}(k)|], \quad (19)$$

where, $E_n^{(s)}(k)$ and $E_n^{(0)}(k)$ are the eigen-energy spectra of the superfluid state and normal state. Here, we focus on the filling lying in the band splitting around the M point induced by the orbital hybridization as shown in Fig. 2(a). The typical Fermi surface is shown in Fig. 2(b). From Eq. (18), we can find that the superfluid order parameter in the intra- p_x orbital channel is $\Delta_{22} = U\Delta_{s,xx} + J_\Delta\Delta_{s,yy}$ while the superfluid order parameter in the intra- p_y orbital channel is $\Delta_{33} = U\Delta_{s,yy} + J_\Delta\Delta_{s,xx}$. To maximize the superfluid gap, one can find that $\Delta_{s,xx}\Delta_{s,yy} > 0$ is favorable to obtain the largest amplitudes of Δ_{22} and Δ_{33} . The numerical results for the ground state energy and superfluid order parameters as functions of chemical potential μ_0 and interaction amplitude $|U|$ are shown in Figs. 2(c) and 2(d), from which the intra-orbital Δ_{22} and Δ_{33} are degenerate in the whole parameter regime. It means that $\Delta_{22} = \Delta_{33}$, and the only choice is $\Delta_{s,xx}\Delta_{s,yy} > 0$ thanks to $UJ_\Delta > 0$. The aforementioned analyses are consistent, and one can achieve that the superfluid ground states favor $\Delta_{s,xx}$ and $\Delta_{s,yy}$ with same sign to maximize the superfluid gap and to minimize the ground state energy. Furthermore, we can find that the inter-orbital Δ_{23} , which is also the matrix element in Eq. (18), is purely imaginary, and much smaller than $\Delta_{22/33}$. The reason lies in that the inter-orbital Δ_{23} is induced by the orbital hybridization and modulated by Ω_z . It is conceivable that the strength of inter-orbital Δ_{23} could be comparable to intra-orbital $\Delta_{22/33}$ when Ω_z is large enough. However, the Δ_{23} has no relation with the topological nature of the superfluid state, we only focus on the case with Ω_z set here.

In order to reveal the underlying topological nature of the superfluid states, we first investigate the band characteristics of the normal states. As shown in Fig. 1(e), the full separation between the d band and p bands guarantees the feasibility to downfold the Hamiltonian from the space spanned by d and p orbitals to the space spanned by two effective \tilde{p} orbitals shown in Fig. 1(f). When $V_t = 0$, the translation symmetry allows ones to write the TB Hamiltonian in momentum space under the effective basis $\tilde{\psi}_\sigma(k) = [\tilde{p}_{x,k,\sigma}, \tilde{p}_{y,k,\sigma}]^t$, i.e.,

$$\tilde{H}_{tb} = \sum_{k\sigma} \tilde{\psi}_\sigma^\dagger(k) \tilde{H}_{tb}(k) \tilde{\psi}_\sigma(k). \quad (20)$$

Here,

$$\tilde{H}_{tb}(k) = \frac{1}{2}\xi_+(k) - \mu_0 + \xi_{xy}(k)\sigma_x - \hbar\Omega_z\sigma_y + \frac{1}{2}\xi_-(k)\sigma_z, \quad (21)$$

and

$$\xi_\pm(k) = 2(\tilde{t}_{pp} \mp \tilde{t}_{pp}')(\cos k_x \pm \cos k_y), \quad (22)$$

$$\xi_{xy}(k) = 4\tilde{t}_{xy} \sin k_x \sin k_y. \quad (23)$$

The Pauli matrices σ_i with $i = x, y, z$ span the two effective \tilde{p}_x and \tilde{p}_y orbital space. The effective TB Hamiltonian \tilde{H}_{tb} can be rewritten in the basis spanned by the orbital angular momentum eigen-state, i.e.,

$$\bar{H}_{tb} = \sum_{k\sigma} \bar{\psi}_\sigma^\dagger(k) \bar{H}_{tb}(k) \bar{\psi}_\sigma(k). \quad (24)$$

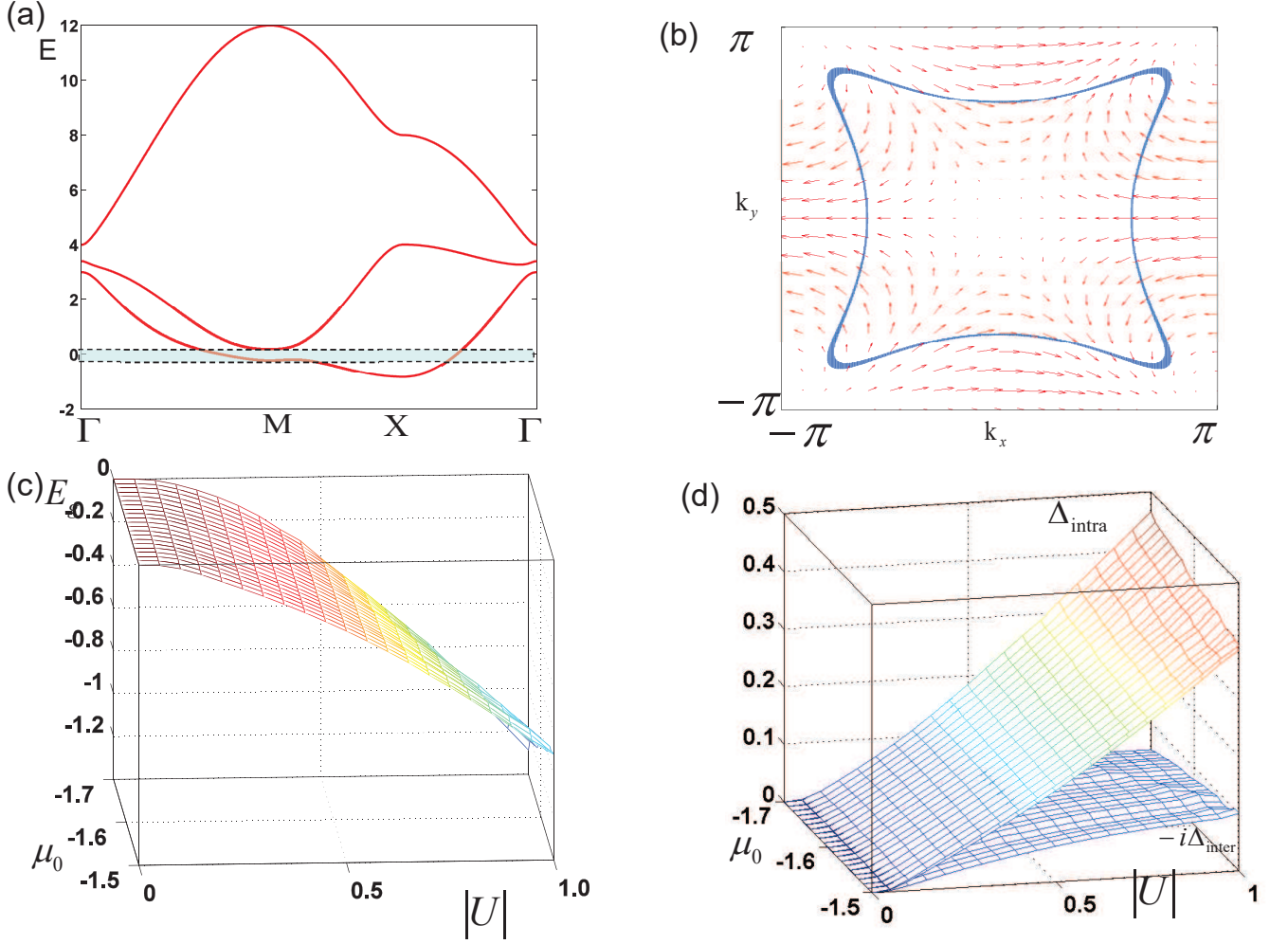


FIG. 2: (Color Online) (a) The band structure along the high-symmetry lines, and the filling is in the shadowed regime by tuning the chemical potential. (b) The closed curve denotes the single Fermi surface. The red arrows denote the vector field of $[\xi_-(k), \xi_{xy}(k)]$. Here, the parameters are same as these in Fig. 1(f). (c) The zero-temperature ground-state energy of superfluid state as change as chemical potential μ_0 and interaction amplitude $|U|$. (d) The intra-and inter-orbital superfluid order parameters as change as chemical potential μ_0 and interaction amplitude $|U|$. Here, $\Delta_{intra} = \Delta_{22}$ with $\Delta_{33} = \Delta_{22}$, and $\Delta_{inter} = \Delta_{23}$. The explicit expressions of Δ_{22} , Δ_{23} and Δ_{33} are shown in Eq.(18), which are the relevant matrix elements. The mesh of $k_x \times k_y = 51 \times 51$.

Here, $\bar{\psi}_\sigma^\dagger(k) = [\bar{p}_{+,k,\sigma}^\dagger, \bar{p}_{-,k,\sigma}^\dagger]$ with $\bar{p}_{\pm,k,\sigma}^\dagger = \frac{1}{\sqrt{2}}[\bar{p}_{x,k,\sigma}^\dagger \pm i\bar{p}_{y,k,\sigma}^\dagger]$, and

$$\bar{H}_{tb}(k) = \frac{1}{2}\xi_+(k) - \mu_0 + \frac{1}{2}\xi_-(k)s_x + \xi_{xy}(k)s_y - \hbar\Omega_z s_z. \quad (25)$$

The Pauli matrices s_i with $i = x, y, z$ span the two effective \bar{p}_+ and \bar{p}_- orbital space. In the absence of Ω_z , $[F_x(k) = \frac{1}{2}\xi_-(k), F_y(k) = \xi_{xy}(k)]$ forms a vector field in momentum space shown in Fig. 2(b). Then, the band degeneracy point at the M point can be mapped into a vortex in the momentum space with integer winding number⁵, i.e.,

$$W_\sigma = \oint \frac{d\mathbf{k}}{2\pi} \left[\frac{F_x(k)}{F(k)} \nabla \frac{F_y(k)}{F(k)} - (x \longleftrightarrow y) \right], \quad (26)$$

with $F(k) = \sqrt{F_x^2(k) + F_y^2(k)}$. The direct calculation gives $W_\sigma = 2$ in agreement with the pattern of the vector field $[F_x(k), F_y(k)]$ as shown in Fig. 2(b). Note that the total winding number $W = W_\uparrow + W_\downarrow$ should be 4 when the spin degree of freedom is taken into account. In the presence of Ω_z , the induced orbital hybridization lifts the degeneracy at M point. Then, the above mapping does not work.

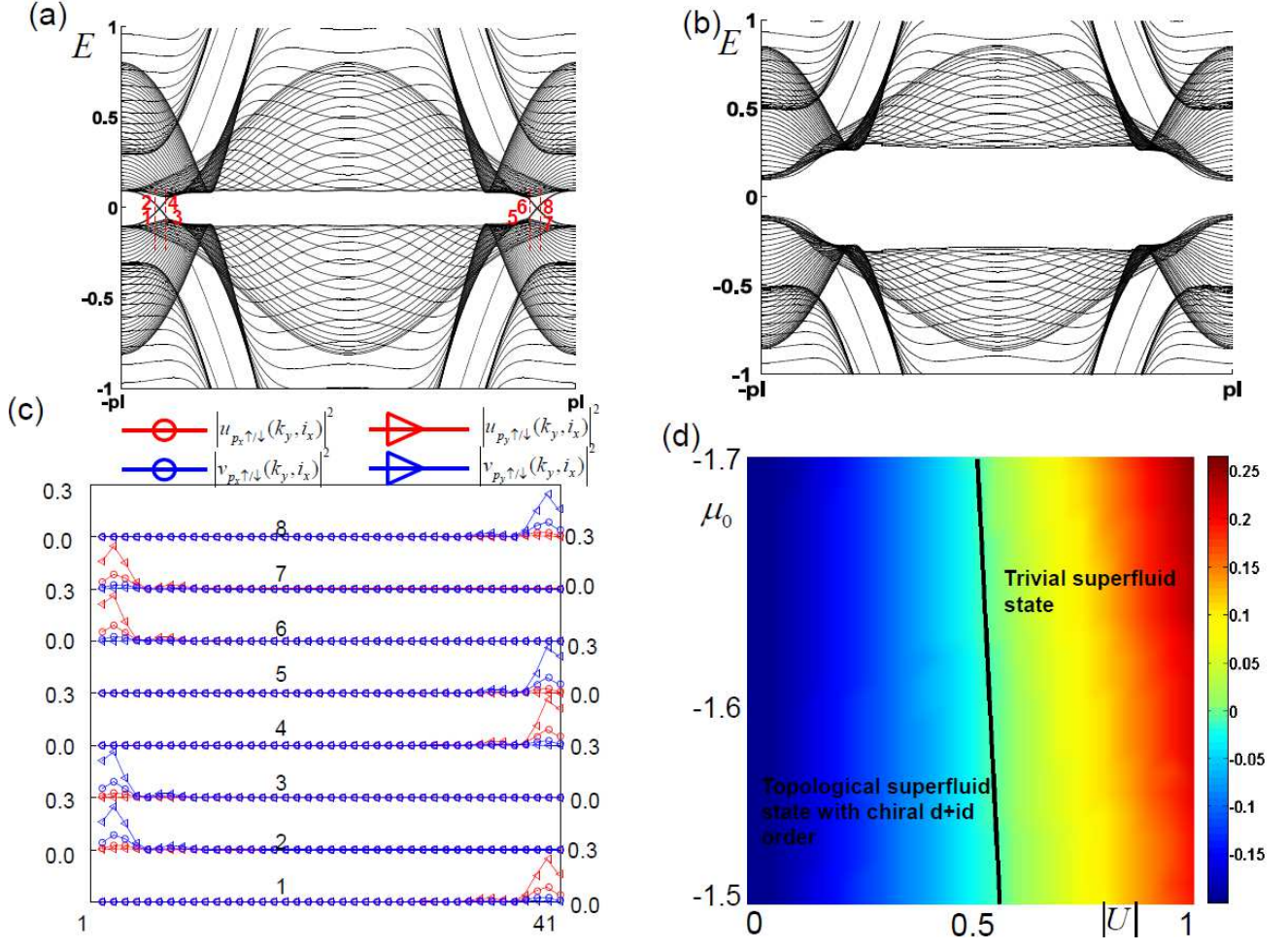


FIG. 3: (Color Online) (a) and (b) the edge spectra of the superfluid states with $|U| = 0.4$, $\mu_0 = -1.6$ in (a) and $|U| = 0.8$, $\mu_0 = -1.6$ in (b). The relevant $\Delta_{intra} = 0.1$, $\Delta_{inter} = 0.03i$ in (a) and $\Delta_{intra} = 0.3$, $\Delta_{inter} = 0.08i$ in (b). Here, the y direction has periodic boundary condition while the lattice number along x direction is set to be $N_x = 41$. (c) The amplitudes of wave-function of the in-gap states labeled 1-8 in (a). Note that each point are double degeneracy by taking into account the spin degree of freedom. Here, the red and blue “o” marks label particle-like $|u_{p_x, \uparrow/\downarrow}(k_y, i_x)|^2$ and hole-like $|v_{p_x, \uparrow/\downarrow}(k_y, i_x)|^2$ while the red and blue “<” marks label particle-like $|u_{p_y, \uparrow/\downarrow}(k_y, i_x)|^2$ and hole-like $|v_{p_y, \uparrow/\downarrow}(k_y, i_x)|^2$. (d) The phase diagram as change as chemical potential μ_0 and interaction amplitude $|U|$.

In the superfluid states, quasi-particle spectra are fully gapped and the nonzero Ω_z breaks the pseudo-time-reversal symmetry. It is natural to introduce the Chern number to characterize the topological properties of the superfluid states. To show it, we consider the effective superfluid Hamiltonian spanned in the effective Nambu basis: $\bar{\Psi}(k) = [\bar{p}_{+,k,\uparrow}, \bar{p}_{-,k,\uparrow}, \bar{p}_{+,-k,\downarrow}^\dagger, \bar{p}_{-,-k,\downarrow}^\dagger, \bar{p}_{+,k,\downarrow}, \bar{p}_{-,k,\downarrow}, \bar{p}_{+,-k,\uparrow}^\dagger, \bar{p}_{-,-k,\uparrow}^\dagger]^t$,

$$\bar{H}_{mf} = \sum_k \bar{\Psi}^\dagger(k) [\bar{H}_{tb}(k) + \bar{H}_{int}^p(k)] \bar{\Psi}(k), \quad (27)$$

with

$$\bar{H}_{int}^p(k) = s_z \otimes \begin{bmatrix} \bar{\Delta} & \bar{\Delta} \\ \bar{\Delta}^\dagger & \bar{\Delta} \end{bmatrix}, \quad (28)$$

and

$$\bar{\Delta} = \begin{bmatrix} |\Delta_{inter}| & \Delta_{intra} \\ \Delta_{intra} & -|\Delta_{inter}| \end{bmatrix}.$$

Here $\Delta_{intra} = \Delta_{22}$ and $|\Delta_{inter}| = |\Delta_{23}|$. Upon an unitary rotation²⁶, we can obtain a dual form of the Hamiltonian, i.e.,

$$\bar{H}_{mf}^D = S \bar{H}_{mf} S^\dagger, \quad (29)$$

where

$$S = \frac{1}{\sqrt{2}} \begin{bmatrix} 1 & s_x & & \\ is_y & -s_z & & \\ & & 1 & -s_x \\ & & -is_y & -s_z \end{bmatrix}, \quad (30)$$

$$\bar{H}_{mf}^D(k) = \begin{bmatrix} \bar{H}_{mf}^{D+}(k) & \\ & \bar{H}_{mf}^{D-}(k) \end{bmatrix}$$

$$\bar{H}_{mf}^{D\pm}(k) = \begin{bmatrix} \Delta_{intra} - h\Omega_z s_z & \pm h(k) \\ \pm h^\dagger(k) & -\Delta_{intra} + h\Omega_z s_z \end{bmatrix}, \quad (31)$$

$$h(k) = is_y \left[-\frac{\xi_+(k)}{2} + \mu_0 + \frac{\xi_-(k)}{2} s_x \right. \\ \left. - \xi_{xy}(k) s_y + is_y |\Delta_{inter}| \right]. \quad (32)$$

In the dual Hamiltonian $\bar{H}_{mf}^{D\pm}(k)$ shown in Eq. (31), $[\frac{\xi_-(k)}{2}, \xi_{xy}(k)]$ resembles two components of pairing order parameters of the chiral d -wave superfluid and Δ_{inter} corresponds to the mixed s -wave component. “ $\Delta_{intra} \pm h\Omega_z$ ” is the pseudo-kinetic energy with k -independent, and resembles kinetic energy term “ $\frac{k^2 \pm k_F^2}{2m}$ ” of the chiral d -wave superfluid when μ_0 is set to satisfy the condition $\mu_0 = \frac{1}{2}\xi_+(\pi, \pi)$. Then, the dual Hamiltonian $\bar{H}_{mf}^{D\pm}(k)$ resembles the standard Hamiltonian describing the chiral d -wave superconductors^{30,44}, and belongs to class C according to the classification by Schnyder *et al*⁴⁵. Here, Δ_{inter} by itself cannot drive the gap-closing condition, because it is much smaller than Δ_{intra} and Fermi energy. Therefore, the small Δ_{inter} can be absorbed and set to zero. The topological nontrivial superfluid states can be achieved under the condition⁴⁴ $\Delta_{intra} < h\Omega_z$ when $\mu_0 = \frac{1}{2}\xi_+(\pi, \pi)$, which naturally corresponds to the weak-coupling condition $\frac{k^2 - k_F^2}{2m} < 0$ ³⁴. For the general case with arbitrary μ_0 , one can obtain nontrivial superfluid states if $f(\Omega_z, \mu_0, \Delta_{intra}) > 0$ with $f(\Omega_z, \mu_0, \Delta_{intra})$ shown in Eq.(33), and trivial superfluid states if $f(\Omega_z, \mu_0, \Delta_{intra}) < 0$. The topological phase transition condition coincides with the gap-closing condition with $f(\Omega_z, \mu_0, \Delta_{intra}) = 0$. The phase diagram separating the topological trivial and non-trivial superfluid phases is plotted in Fig. 3(d) according to phase transition condition $f(\Omega_z, \mu_0, \Delta_{intra}) = 0$.

$$f(\Omega_z, \mu_0, \Delta_{intra}) = |h\Omega_z| - \sqrt{\Delta_{intra}^2 + \left[\frac{\xi_+(\pi, \pi)}{2} - \mu_0 \right]^2}. \quad (33)$$

The nontrivial topological nature of the superfluid states can be characterized by the Chern number,

$$\mathcal{C}_s = \frac{i}{2\pi} \sum_{E_n < 0} \int_{BZ} d\mathbf{k} \langle \nabla_k u_{s,n}(\mathbf{k}) | \times | \nabla_k u_{s,n}(\mathbf{k}) \rangle, \quad (34)$$

with $u_{s,n}(\mathbf{k})$ the Bloch functions of occupied quasi-particle states with $s = up$ and $down$ to label the the up-block and down-block parts of Hamiltonian in Eq. (17). The straightforward calculations give $\mathcal{C}_{up} = \mathcal{C}_{down} = 2$ for $h\Omega_z > 0$ and $\mathcal{C}_{up} = \mathcal{C}_{down} = -2$ for $h\Omega_z < 0$ under the condition $f(\Omega_z, \mu_0, \Delta_{intra}) > 0$, which means the inverse local rotation corresponds to reverse chirality. From the bulk-edge correspondence, the quasi-particle spectra have two chiral gapless edge states at the open boundary shown in Fig. 3(a) and no gapless edge states emerge in trivial superfluid state shown in Fig.3(b). The local feature of the edge states in the Fig. 3(a) are explicitly demonstrated through the amplitude distributions of the wave-functions shown in Fig. 3(c).

IV. MASS DENSITY MODULATION FROM THE HARMONIC CONFINING POTENTIAL

Now, we consider the realistic case with nonzero harmonic confining potential in Eq. (8), and the pattern of $V_{trap}(i_x, i_y)$ is shown in Fig. 4(a) with $V_t = 1.2/N_x N_y$. We perform the self-consistent calculations about the Bogoliubov-de Gennes (BdG) Hamiltonian $H_{tb} + H_{int}^p$ in Eqs. (4) and (15) in lattice space. The quasi-particle spectra and the distribution of superfluid order

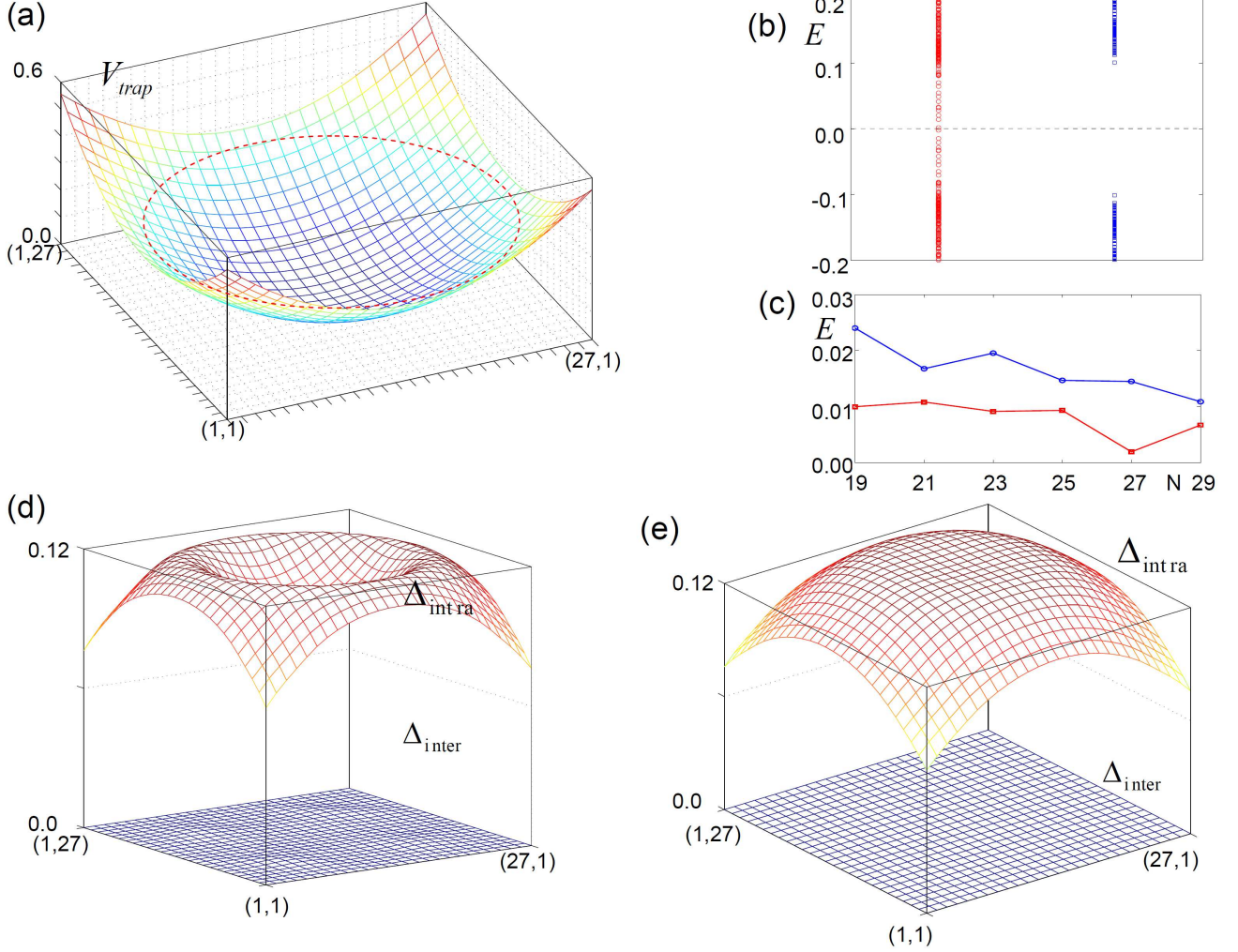


FIG. 4: (Color Online) (a) The pattern of weak harmonic confining potential V_{trap} with $V_t = 1.2/N_x N_y$ in lattice space. The red-dashed circle denotes a spacial barrier structure of the potential, which separates the two different superfluid states. (b) The spectra of the superfluid states with the red “o” marks and the blue “□” marks corresponding to the case with $\hbar\Omega_z = 0.2$ and $\hbar\Omega_z = 0.05$ respectively. (c) The energy levels of the in-gap fermion zero modes as function of lattice size $N \times N$. Here, the red “□” marks and the blue “o” marks correspond to the first and second lowest positive energy levels, and $\hbar\Omega_z = 0.2$. (d) and (e) The distributions of superfluid order parameters including intra-orbital and inter-orbital parts in lattice space with lattice size $(N_x, N_y) = (27, 27)$ and $\hbar\Omega_z = 0.2$ in (c) and $\Omega_z = 0.05$ in (d). Here, the interaction strength $|U| = 0.8$, chemical potential $\mu_0 = -1.6$, and the periodic boundary condition is applied. Other parameters are same as those in Fig. 1.

parameters are shown in Figs. 4(b), 4(d), and 4(e) for two different $\hbar\Omega_z = 0.2$ and $\hbar\Omega_z = 0.05$ under the periodic boundary condition. We find that the amplitudes of superfluid order parameters in both cases are similar from Fig. 4(d) and 4(e), but the quasi-particle spectra are quite different from Fig. 4(b) with in-gap fermion modes for $\hbar\Omega_z = 0.2$ and without in-gap fermion modes for $\hbar\Omega_z = 0.05$. The reason lies in that $V_{trap}(i_x, i_y)$ forms a spatial barrier structure [The position is marked with red-dashed circle in Fig. 4(a)] separating the nontrivial superfluid state with $f(\Omega_z, \mu_i, \Delta_{intra}) > 0$ and trivial superfluid state with $f(\Omega_z, \mu_i, \Delta_{intra}) < 0$ for $\Omega_z = 0.2$. Note that $\mu_i = \mu_0 + V_{trap}(i_x, i_y)$, thus the position of spatial barrier coincides with the gap-closing condition with $f(\Omega_z, \mu_i, \Delta_{intra}) = 0$. For fixed μ_0 and V_t , one can find that $f(\Omega_z, \mu_i, \Delta_{intra})$ is always smaller than zero when $\Omega_z = 0.05$. The superfluid is always trivial, because $\Omega_z = 0.05$ is too small to overcome the gap-closing condition $f(\Omega_z, \mu_i, \Delta_{intra}) = 0$. The spatial barrier traps in-gap fermion modes and accumulates atoms when the negative energy states are occupied^{44,46}. The in-gap fermion modes trapped by the spatial barrier have the same origin as the fermion modes in spectrum of the Caroli-de Gennes-Matricorn bound states in the vortex core⁴⁷.

In the low-energy limit, the spectrum of in-gap fermion modes in terms of the angular momentum Q takes the following form

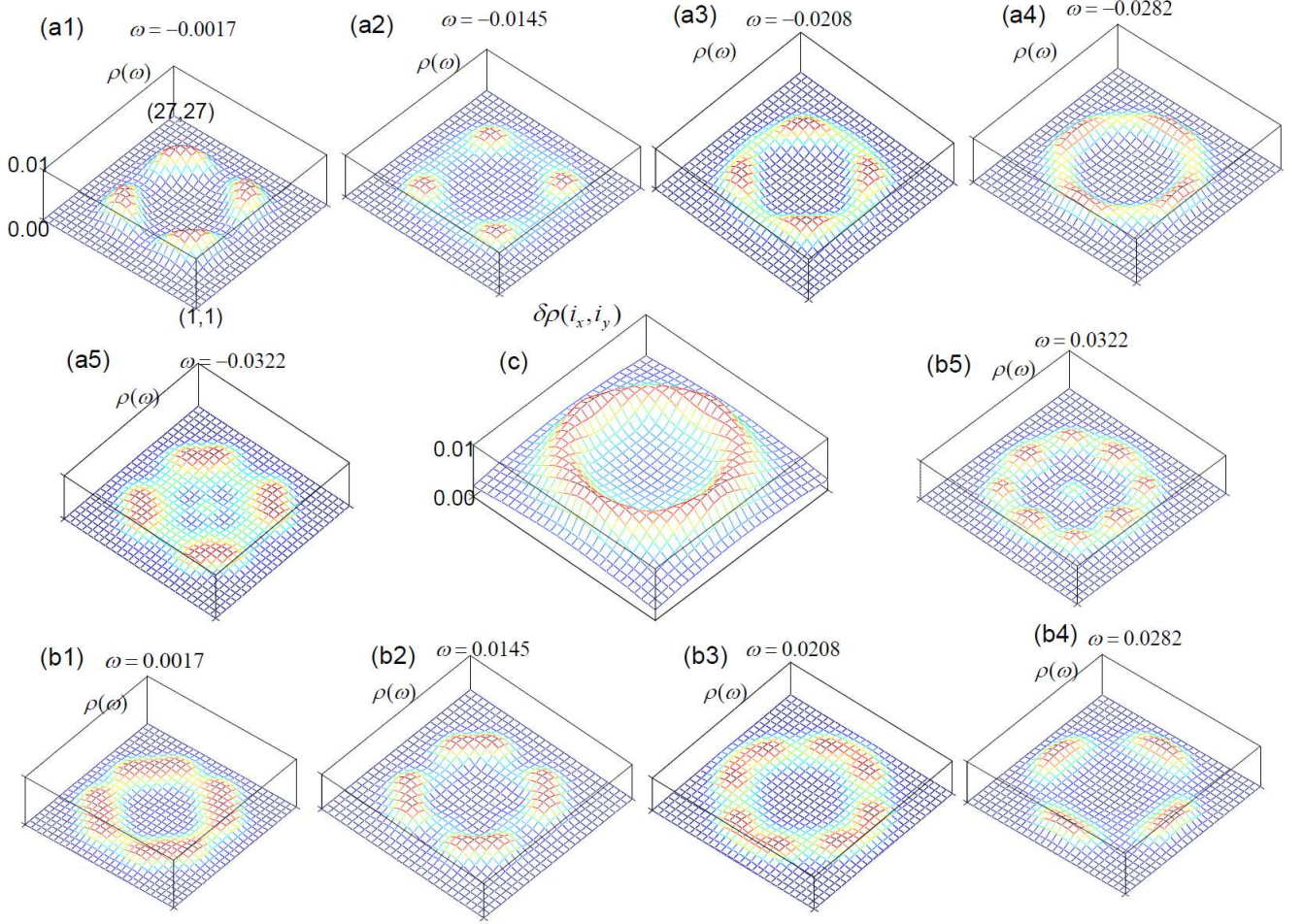


FIG. 5: (Color Online) (a1)-(a5) The distribution of LDOS defined in Eq. (36) for five fermion modes with negative energy close to zero. (b1)-(b5) The distribution of LDOS defined in Eq. (36) for five fermion modes with positive energy close to zero. (c) The distribution of change of LDOS between $\hbar\Omega_z = 0.2$ and $\hbar\Omega_z = 0.22$. Here, the parameters are same as those in Fig. 4.

under the axisymmetric condition^{44,46},

$$E_a(Q) = \omega_a(Q - Q_a), \quad (35)$$

where $\omega_a = c_a/R$ is the angular velocity of the rotation along the spatial barrier with R the radius of spatial barrier of $V_{trap}(i_x, i_y)$ ⁴⁸, a labels the a th branch, and $Q_a = \hbar k_a R$. The total number of the branches is four according to the index theorem⁴⁶ when the spin degree of freedom is taken into account. In the absence of external driving, the energy of in-gap fermion modes is $E_a(0) = -\omega_a Q_a$. In the square lattice space, the circular rotation symmetry $SO(2)$ for Eq. (35) is broken down to C_4 symmetry, and the Fermi velocity is strongly anisotropic and the superfluid order parameters are highly inhomogeneous. Q_a can only take the discrete values under the constraint of C_4 symmetry. Correspondingly, the energy levels of the in-gap fermion modes trapped by the spatial barrier are discrete [see Fig. 4(b) for details], and several energy levels close to zero usually correspond to in-gap fermion modes trapped by the spatial barrier.

The localization feature of the in-gap fermion modes trapped by the spatial barrier can be reflected by the local density of states (LDOS), which is calculated by

$$\rho_i(\omega) = \sum_{n,l,\sigma} [|u_{i,l\sigma}^n|^2 \delta(E_n - \omega) + |v_{i,l\sigma}^n|^2 \delta(E_n + \omega)], \quad (36)$$

where $u_{i,l\sigma}^n$ and $v_{i,l\sigma}^n$ are the particle-like and hole-like components of eigenstate with quasi-particle energy E_n at site i and orbital l . The LDOS of the five in-gap fermion modes with the highest negative energy are shown in Fig. 5(a1)-(a5), from which we can find that four levels with energy -0.0017 , -0.0145 , -0.0208 , -0.0282 are the fermion modes which are trapped by the spatial barrier. To make a comparison, the level with energy -0.0322 is the extended state. We also plot the LDOS of the five levels with the lowest positive energy in Fig. 5(b1)-(b5) for comparison. Furthermore, we find that the highest negative energy level and the lowest positive energy level approach zero energy with increasing the lattice size $N \times N$ [see Fig. 4(c) for details].

In the presence of external driving, the spectrum of the in-gap fermion modes is a function of the angular momentum Q from the external driving, and the in-gap fermion modes could cross the zero energy and form the variation of the mass current. The change of the mass current trapped in the spatial barrier is⁴⁴

$$\delta I_M = \frac{\hbar}{8\pi} \sum_a \delta(k_a^2), \quad (37)$$

where we have assumed the thickness along z direction to be unity. The extra $1/2$ in denominator is added to compensate the double count due to the particle-hole symmetry. Generally, there are several external perturbations which can be introduced to be the driving force to move the in-gap fermion modes cross the zero energy, such as the modulations of V_1 and V_2 in Eq. (1) to deform the $\frac{\xi_-(k)}{2}$ and $\xi_{xy}(k)$ and introducing additional laser beam to modulation the trapping potential. Here, we consider a more convenient method. From Eq. (35), it is straightforward to inject non-zero Q into the superfluid state through slight modulation of local rotating frequency Ω_z . As a consequence, the in-gap fermion modes can be driven to cross the zero energy by the non-zero $\delta\Omega_z$. If we further assume that all the in-gap fermion modes trapped in the spatial barrier have the relation $\frac{\hbar^2 \delta(k_a^2)}{2m} \sim \hbar \delta\Omega_z$, we can obtain that the response of change of mass current to the modulation of the rotating frequency $\delta I_M \sim \frac{m \delta\Omega_z}{2} \sum_a \text{sgn}(c_a)$ with the summation involving all the in-gap fermion modes cross zero energy. However, in the square lattices, we can find that the k_a is different for different a -th branch from Fig. 5. As a good approximation, we can define an effective $\langle k \rangle$ to remove the difference of different k_a , and $\langle k \rangle$ can be replaced with the average Fermi momentum $\langle k_F \rangle$. Then, we can obtain that the modulation of mass current density is proportional to the change of the LDOS, i.e.,

$$\delta j_M(i_x, i_y) \propto \delta \rho(i_x, i_y), \quad (38)$$

with

$$\delta \rho(i_x, i_y) = \rho(i_x, i_y)|_{\Omega_z + \delta\Omega_z} - \rho(i_x, i_y)|_{\Omega_z}, \quad (39)$$

$$\rho(i_x, i_y)|_{\Omega_z} = \sum_{n,l,\sigma} |v_{l\sigma}^n(i_x, i_y)|^2 \theta(-E_n)|_{\Omega_z}. \quad (40)$$

The pattern of $\delta \rho(i_x, i_y)$ for $\delta\Omega_z = 0.02/h$ is shown in Fig. 5(c), from which we can find that the mass current is trapped around the spatial barrier.

V. DISCUSSIONS AND CONCLUSIONS

In terms of experiment, the fermion atoms can be selected as lithium ^6Li , two internal states can be selected as $^2\text{S}_{1/2}$ with $M=\pm\frac{1}{2}$. The principal fluorescence line from $^2\text{S}_{1/2}$ to ^2P is at 670.8 nm. Therefore, a Nd:YAG-laser with 532 nm could be selected to be the light source to realize the optical potential with the lattice constant $a = 532$ nm. The recoil energy $E_R \sim \hbar \times 100$ KHz. The local rotation around each potential minimum has been experimentally realized through inserting electrooptic phase modulators into the beams forming the 2D lattice potential, and the relevant rotating frequency Ω_z can be turned with large flexibility¹⁸. From the energy bands in Fig. 1, we can estimate that it is enough for $\Omega_z \sim \hbar \times 2$ KHz to satisfy the topological superfluid condition.

In the presence of the harmonic trap, it has been shown that the local density approximation(LDA) breaks down for trapped non-interacting bosons in p-orbital bands, and increasing the interactions and optical lattice potentials can suppress anisotropy of condensate density⁴⁹. However, the picture is different for trapped non-interacting fermions in p-orbital bands due to the different statistics. It is shown that the hard-core boson known as Tonks-Girardeau boson with infinitely repulsive interactions can be mapped into non-interacting free fermion in one dimensional limit⁵⁰⁻⁵². Thus, the boson with infinitely repulsive interactions is roughly equivalent to free fermion even in two dimensional system. Such effective “repulsive interactions” can suppress the anisotropy of condensate density, and guarantee the validity of LDA in system with trapped fermions in p-orbital bands. Furthermore, the tunability of the optical lattice potential and quite small trap potential can further reduce the anisotropy of

condensate density. Though the breaking down of LDA can be suppressed, the particle density per site will inevitably vary and the s-orbital atoms will thereby shift the onsite energies for p-orbital atoms in the presence of the trap. Thanks to the small trap potential, one can expect that the density fluctuations of the both trapped s-orbital and p-orbital atoms should be small, and the main results throughout the paper are not changed qualitatively.

The change of the mass current and the accumulation of the atoms around the spatial barrier can be spatially resolved with the radio-frequency spectroscopy⁵³⁻⁵⁵. Besides the radio-frequency spectroscopy, the recently developed matter-wave interference technique⁵⁶ is a more powerful tool, which can directly represent the phase properties of the superfluid order parameter. More remarkably, one can reconstruct the spatial geometry of certain low-energy in-gap fermion modes and verify the formation of the spatial barrier structure, both of which are the key signatures in our proposal.

In summary, we propose that the superfluid states of fermions with a chiral d -wave order can be implemented in a rotating optical lattice where the orbital degrees of freedom play a key role. Our proposal presents an alternative route to realize the topological superfluids with chiral even-frequency order in the absence of the spin-orbital coupling. Furthermore, we show that the intrinsic harmonic confining potential can form a circular spatial barrier structure which accumulates atoms and support a mass current under the injection of small angular momentum as driving force. The mass current associated with the accumulated atoms can be experimentally detected, and provides a signature to verify the emergence of topological superfluid state with chiral d -wave order in a rotating optical lattice.

Acknowledgments

We thank S.-Q. Shen, S. Z. Zhang, D. W. Zhang, G. C. Liu for useful discussions. This work was supported by NSFC under Grants No. 11674331, No. 11274032, No.11625415, the Ministry of Science and Technology of China (Grant number: 2017YFA0303200), and by 100 Talents Programme of CAS.

* Electronic address: haon@hmfl.ac.cn

† Electronic address: zhang_ping@iapcm.ac.cn

¹ Müller T, Fölling S, Widera A, and Bloch I 2007 *Phys. Rev. Lett.* **99**, 200405

² Wirth G, Ölschläger M, and Hemmerich A 2011 *Nat. Phys.* **7**, 147

³ Soltan-Panahi P, Luhmann D-S, Struck J, Windpassinger P, and Sengstock K 2012 *Nat. Phys.* **8**, 71

⁴ Parker C V, Ha L-C, and Chin C 2013 *Nat. Phys.* **9**, 769

⁵ Sun K, Liu W V, Hemmerich A, and Sarma S D 2012 *Nat. Phys.* **8**, 67

⁶ Li X, Zhao E, and Liu W V 2013 *Nat. Commun.* **4**, 1523

⁷ Liu B, Li X, Wu B, and Liu W V 2014 *Nat. Commun.* **5**, 5064

⁸ Liu B, Li X, and Liu W V 2015 *arXiv:1505.07444*

⁹ Wu C 2008 *Phys. Rev. Lett.* **100**, 200406

¹⁰ Wu C 2008 *Phys. Rev. Lett.* **101**, 186807

¹¹ Zhai Y *et al* 2013 *Phys. Rev. A* **87**, 063638

¹² Qi X-L and Zhang S-C 2011 *Rev. Mod. Phys.* **83**, 1057

¹³ Hasan M Z and Kane C L 2010 *Rev. Mod. Phys.* **82**, 3045

¹⁴ Struck J *et al* 2011 *Science* **333**, 996. Weinberg S M *et al* 2013 *Nat. Phys.* **9**, 738. Struck J *et al* 2012 *Phys. Rev. Lett.* **108**, 225304

¹⁵ Hauke P *et al* 2012 *Phys. Rev. Lett.* **109**, 145301

¹⁶ Parker C V, Ha L-C, and Chin C 2013 *Nat. Phys.* **9**, 769

¹⁷ Koghee S, Lim L K, Goerbig M O, and Smith C M 2012 *Phys. Rev. A* **85**, 023637

¹⁸ Gemelke N, Sarajlic E, and Chu S 2010 *arXiv:1007.2677*

¹⁹ Pinheiro F *et al* 2013 *Phys. Rev. Lett.* **111**, 205302

²⁰ Zhang S-L and Zhou Q 2014 *Phys. Rev. A* **90**, 051601

²¹ Zheng W, and Zhai H 2014 *Phys. Rev. A* **89**, 061603

²² Ölschläger M, Wirth G, and Hemmerich A 2011 *Phys. Rev. Lett.* **106**, 015302

²³ Ölschläger M, Kock T, Wirth G, Ewerbeck A, Smith C M, Hemmerich A 2013 *New Journal of Physics* **15**, 083041

²⁴ Chin C, Grimm R, Julienne P, and Tiesinga E 2010 *Rev. Mod. Phys.* **82**, 1225

²⁵ Zhang C, Tewari S, Lutchyn R M, and Sarma S D 2008 *Phys. Rev. Lett.* **101**, 160401

²⁶ Sato M, Takahashi Y, and Fujimoto S 2009 *Phys. Rev. Lett.* **103**, 020401

²⁷ Liu G, Hao N, Zhu S-L, and Liu W-M 2012 *Phys. Rev. A* **86**, 013639

²⁸ Hao N, Liu G, Wu N, Hu J, and Wang Y 2013 *Phys. Rev. A* **87**, 053609

²⁹ Krishana K, Ong N P, Li Q, Gu G D, Koshizuka N 1997 *Science* **277**, 83

³⁰ Laughlin R B 1998 *Phys. Rev. Lett.* **80**, 5188

³¹ Nandkishore R, Levitov L S, and Chubukov A V 2012 *Nat. Phys.* **8**, 158

³² Liu F, Liu C-C, Wu K, Yang F, and Yao Y 2013 *Phys. Rev. Lett.* **111**, 066804

- ³³ Zhang S, Lang L and Zhou Q 2015 *Phys. Rev. Lett.* **115**, 225301
- ³⁴ Read N and Green D 2000 *Phys. Rev. B* **61**, 10267
- ³⁵ Fu L, and Kane C L 2008 *Phys. Rev. Lett.* **100**, 096407
- ³⁶ Sau J D, Lutchyn R M, Tewari S, and Sarma S D 2010 *Phys. Rev. Lett.* **104**, 040502
- ³⁷ Mao L, Shi J, Niu Q, and Zhang C 2011 *Phys. Rev. Lett.* **106**, 157003
- ³⁸ Wang Z, Hao N, Fu Z G, and Zhang P 2012 *New Journal of Physics* **14**, 063010
- ³⁹ Hao N, Zhang P, Li J, Wang Z, Zhang W, and Wang Y 2010 *Phys. Rev. B* **82**, 195324
- ⁴⁰ Shen S Q 2012 *Topological insulators* (Springer, Berlin)
- ⁴¹ Zhang S, Hung H H, and Wu C 2010 *Phys. Rev. A* **82**, 053618
- ⁴² Collin A, Larson J, and Martikainen J-P 2010 *Phys. Rev. A* **81**, 039905
- ⁴³ Sowinski T *et al* 2013 *Phys. Rev. Lett.* **111**, 215302
- ⁴⁴ Volovik G E 1997 *JETP Lett.* **66**, 522-527
- ⁴⁵ Schnyder A P, Ryu S, Furusaki A, and Ludwig A W W 2008 *Phys. Rev. B* **78**, 195125
- ⁴⁶ Volovik G E 2003 *The universe in a helium droplet* (Oxford University Press)
- ⁴⁷ Caroli C, Gennes P G D, and Matricon J 1964 *Phys. Lett.*, **9**, 307
- ⁴⁸ Unlike the vortex case, where the radius of vortex has the same order of coherence length $\xi \sim v_F/\Delta_0$, the domain wall could collapse when $R \sim \xi$. Thus, the V_i should not be too large to have large R . Here, we have $R \sim 10a$ for $V_i = 1.2/N_x N_y$, and R is much larger than $\xi \sim 3a$ if the v_F is estimated from the Fermi energy along $\Gamma - M$ direction.
- ⁴⁹ Pinheiro F, Martikainen J-P, and Larson J 2012 *Phys. Rev. A* **85**, 033638
- ⁵⁰ Girardeau M 1960 *J. Math. Phys.* **1**, 516
- ⁵¹ Paredes B *et al* 2004 *Nature (London)* **429**, 277
- ⁵² Kinoshita T *et al* 2004 *Science* **305**, 1125
- ⁵³ Gupta S *et al* 2003 *Science* **300**, 1723
- ⁵⁴ Regal C A, and Jin D S 2003 *Phys. Rev. Lett.* **90**, 230404
- ⁵⁵ Shin Y, Schunck C H, Schirotzek A, and Ketterle W 2007 *Phys. Rev. Lett.* **99**, 090403
- ⁵⁶ Kock T, Ölschläger M, Ewerbeck A, Huang W-M, Mathey L, and Hemmerich A 2015 *Phys. Rev. Lett.* **114**, 115301